

Pion production in intermediate-energy heavy-ion collisions with a relativistic quantum molecular dynamics model

Si-Na Wei* and Zhao-Qing Feng†

School of Physics and Optoelectronics, South China University of Technology, Guangzhou 510640, China

The relativistic mean field approach by distinguishing the slope of symmetry energy is implemented into the Lanzhou quantum molecular dynamics transport model (LQMD.RMF). The collective flows in the isotopic nuclear reactions are systematically investigated by the relativistic quantum molecular dynamics model with various slopes of symmetry energy. The structure of the directed and elliptic flows is consistent with the results of the nonrelativistic transportation of nucleon system. The directed flow difference between free neutrons and protons appears in the midrapidity region. The transverse momentum spectra of π^+ production is close to each other in the nearly symmetric $^{108}\text{Sn} + ^{112}\text{Sn}$ system and the neutron-rich $^{132}\text{Sn} + ^{124}\text{Sn}$ system. However, since there are more neutron-neutron scatterings in neutron-rich system, the transverse momentum spectra of π^- production in the neutron-rich system are higher than one in the nearly symmetric system. For a given reaction system, the transverse momentum spectra of π^+ and π^- production are independent on the stiffness of symmetry energy. This leads to the fact that the single ratio and the double ratio are independent on the stiffness of symmetry energy. Moreover, the double ratio without the π -nucleon potential decreases with increasing the transverse momentum. However, the double ratio with the inclusion of π potential increases with increasing the transverse momentum.

I. INTRODUCTION

The equation of state (EOS) of nuclear matter, which originates from the nucleon-nucleon interaction, plays an important role in heavy-ion collisions and properties of nuclei and neutron star (NS). To extract the nuclear EOS, the heavy-ion collisions, properties of nuclei and NS have been widely studied. Since the nuclear many-body problems are highly nonlinear and the EOS is not a direct observable quantity in experiments, there are still some uncertainties in the EOS after great effort[1–6]. For instance, the EOS of nuclear matter extracted from the data of the heavy-ion collisions still has uncertainties at high nuclear density[1], and the EOS extracted from GW170817 event also has uncertainties at high nuclear density[2]. Although the EOS can be extracted from properties of NS, the internal composition of NS is still poorly understood. The core of NS may contain exotic materials, such as hyperons, kaons, pions and deconfined quark matter[7–11]. The heavy-ion collisions in terrestrial laboratory provide a unique possibility to study both the EOS and exotic materials.

The collective flows of heavy-ion collision were proposed in the 1970's and first detected in experiment at Bevalac[12–15]. Since the collective flows are associated with the nucleon-nucleon interaction, nucleon-nucleon scattering etc, the collective flows have been used to extract the nuclear EOS. The collective flows are also helpful in understanding the phase transition between hadronic matter and quark matter. The collective flows after hadron-quark phase transition would have some differences compared to the collective flows of pure hadronic matter. Generally, when the phase transition between hadronic matter and quark matter occurs, the collective flows of heavy-ion collision indicate

a soft EOS [16–19]. Besides, the ratios of isospin particles in heavy-ion collisions, such as π^-/π^+ , K^0/K^+ and Σ^-/Σ^+ , are though to be sensitive to the isospin asymmetric part of EOS (the nuclear symmetry energy)[20–26]. In experiment, the production of pions and kaons has been measured in $^{197}\text{Au} + ^{197}\text{Au}$ collisions. The K^+ production predicted by various transport model favors a soft EOS at high baryon densities[27–31]. However, the π^-/π^+ ratio predicted by various transport models is still model dependent[32–35]. Based on the FOPI data of the π^-/π^+ ratio[36], some results favor a stiff symmetry energy[32, 33], however, others conclusions imply a soft symmetry energy[34, 35]. Recently, by analysing the ratios of the charged pion in $^{132}\text{Sn} + ^{124}\text{Sn}$, $^{112}\text{Sn} + ^{124}\text{Sn}$ and $^{108}\text{Sn} + ^{112}\text{Sn}$ collisions[37], the slope of the symmetry energy ranging from 42 to 117 MeV was predicted[38]. In different transport models, the relation between the ratios of the charged pion and the properties of symmetry energy may be different. It is still worthwhile to study the ratios of the charged pion in different transport models.

As one of the popular transport models, the quantum molecular dynamics (QMD) approach has been developed into many versions and has been used to describe the heavy-ion collisions successfully. At high-energy heavy-ion collisions, since the relativistic effects become significant, the relativistic effects should be taken account in the QMD. The relativistic QMD (RQMD) approach was proposed in this purpose[39, 40]. Recently, the relativistic mean meson field theory has been implemented into the QMD model (QMD.RMF)[41–43]. The RQMD.RMF has been applied to investigate the collective flows of hadrons successfully[41–43]. In this work, we implement the relativistic mean-field theory with isovector-vector and isovector-scalar fields into the Lanzhou quantum molecular dynamics model (LQMD.RMF) to investigate the collective flows and the ratios of the charged pion. The channel of generation and decay of resonances ($\Delta(1232)$, $N^*(1440)$, $N^*(1535)$, etc), hyperons and mesons has

*Electronic address: Electronic address: 471272396@qq.com

†Electronic address: Corresponding author: fengzhq@scut.edu.cn

been included[31, 32, 44] in the LQMD model. With the LQMD.RMF, we are able to explore the relation between the EOS and the properties of the charged pion.

The paper is organized as follows. In Sec. II, we briefly introduce formulas and approaches used in this work. The formulas include RMF theory, dispersion relation and production of pion. Results and discussions are presented in Sec. III. A summary is finally given in Sec. IV.

II. FORMALISM

A. Relativistic mean field theory

The interaction of RMF is achieved by exchanging mesons. The scalar and vector mesons provide the medium-range attraction and short-range repulsion between the nucleons, respectively[45]. The nonlinear self-interaction of the σ meson is introduced to bring down the incompressibility to a reasonable domain[46]. To investigate the properties of symmetry energy, we also consider the isovector-vector ρ [47] and the isovector-scalar δ mesons[48]. The Lagrangian density is written as

$$\begin{aligned} \mathcal{L} = & \bar{\psi}[\gamma_\mu(i\partial^\mu - g_\omega\omega^\mu - g_\rho\vec{\tau} \cdot \vec{b}^\mu) - (M_N - g_\sigma\sigma \\ & - g_\delta\vec{\tau} \cdot \vec{\delta})]\psi + \frac{1}{2}(\partial_\mu\sigma\partial^\mu\sigma - m_\sigma^2\sigma^2) - \frac{1}{3}g_2\sigma^3 \\ & - \frac{1}{4}g_3\sigma^4 + \frac{1}{2}m_\omega^2\omega_\mu\omega^\mu - \frac{1}{4}F_{\mu\nu}F^{\mu\nu} + \frac{1}{2}m_\rho^2\vec{b}_\mu\vec{b}^\mu \\ & - \frac{1}{4}\vec{B}_{\mu\nu}\vec{B}^{\mu\nu} + \frac{1}{2}(\partial_\mu\vec{\delta} \cdot \partial^\mu\vec{\delta} - m_\delta^2\vec{\delta}^2), \end{aligned} \quad (1)$$

where $M_N = 938$ MeV is the nucleon mass in the free space. g_i with $i = \sigma, \omega, \rho, \delta$ is the coupling constants between the nucleon. m_i with $i = \sigma, \omega, \rho, \delta$ is the meson masses. g_2 and g_3 are the coupling constants of the nonlinear self-interaction of σ meson. $F_{\mu\nu} = \partial_\mu\omega_\nu - \partial_\nu\omega_\mu$ and $\vec{B}_{\mu\nu} = \partial_\mu\vec{b}_\nu - \partial_\nu\vec{b}_\mu$ are the strength tensors of ω and ρ mesons, respectively. The equations of motion for the nucleon and meson are obtained from the Euler-Lagrange equations, and written as

$$[i\gamma^\mu\partial_\mu - g_\omega\gamma^0\omega_0 - g_\rho\gamma^0b_0\tau_3 - (M_N - g_\sigma\sigma - g_\delta\tau_3\delta_3)]\psi = 0 \quad (2)$$

$$m_\sigma^2\sigma + g_2\sigma^2 + g_3\sigma^3 = g_\sigma\bar{\psi}\psi = g_\sigma\rho_S \quad (3)$$

$$m_\omega^2\omega_0 = g_\omega\bar{\psi}\gamma^0\psi = g_\omega\rho \quad (4)$$

$$m_\rho^2b_0 = g_\rho\bar{\psi}\gamma^0\tau_3\psi = g_\rho\rho_3, \quad (5)$$

$$m_\delta^2\delta_3 = g_\delta\bar{\psi}\tau_3\psi = g_\delta\rho_{S3}, \quad (6)$$

where ρ and ρ_S are the baryon and the scalar densities, respectively. $\rho_3 = \rho_p - \rho_n$ is the difference between the proton and neutron densities, and $\rho_{S3} = \rho_{Sp} - \rho_{Sn}$ is

the difference between the proton and neutron scalar densities.

In the RMF approximation, the energy density is given as

$$\begin{aligned} \epsilon = & \sum_{i=n,p} 2 \int_0^{p_F} \frac{d^3p}{(2\pi)^3} \sqrt{p^2 + M_i^2} + \frac{1}{2}m_\sigma^2\sigma^2 + \frac{1}{3}g_2\sigma^3 \\ & + \frac{1}{4}g_3\sigma^4 + \frac{1}{2}m_\omega^2\omega_0^2 + \frac{1}{2}m_\rho^2b_0^2 + \frac{1}{2}m_\delta^2\delta_3^2, \end{aligned} \quad (7)$$

where p_F is the nucleon Fermi momentum. $M_i = M_N - g_\sigma\sigma \mp g_\delta\delta_3$ ($-$ proton, $+$ neutron) is the effective nucleon mass. With the isospin asymmetry parameter $\alpha = (\rho_n - \rho_p)/(\rho_n + \rho_p)$, the symmetry energy is written as[48]

$$\begin{aligned} E_{sym} &= \frac{1}{2} \frac{\partial^2 E(\rho, \alpha)}{\partial \alpha^2} \Big|_{\alpha=0} \\ &= \frac{1}{6} \frac{p_F^2}{E_F^*} + \frac{1}{2} f_\rho \rho - \frac{f_\delta}{2} \frac{M^{*2} \rho}{E_F^{*2} [1 + f_\delta A(p_F, M^*)]} \end{aligned} \quad (8)$$

where $f_i \equiv \frac{g_i^2}{m_i^2}$, $i = \rho, \delta$. $E_F^* = \sqrt{p_F^2 + M^{*2}}$ and $M^* = M_N - g_\sigma\sigma$ is the effective nucleon mass of symmetric nuclear matter. The integral $A(p_F, M^*)$ is defined as

$$\begin{aligned} A(p_F, M^*) &= \frac{4}{(2\pi)^3} \int d^3p \frac{p^2}{(p^2 + M^{*2})^{3/2}} \\ &= 3 \left(\frac{\rho_S}{M^*} - \frac{\rho}{E_F^*} \right). \end{aligned} \quad (9)$$

In this work, we set the saturation density as $\rho_0 = 0.16 \text{ fm}^{-3}$. The binding energy per particle of symmetry nuclear matter is set to be $E/A - M_N = -16$ MeV. For symmetric nuclear matter, we set set1, set2 and set3 models to be the same as a result of vanishing isospin asymmetry. As shown in Table I and Fig.1, the symmetry energy of set1, set2 and set3 is set to be 31.6 MeV at saturation density. The set1 contains only ρ meson, however, set2 and set3 contains both the ρ and δ mesons. For set1, when the symmetry energy is set to be 31.6 MeV at saturation density, the coupling parameters g_ρ is fixed, and the slope of symmetry is fixed to $L = 85.3$ MeV. For set2 and set3, the slope of symmetry energy is obtained by varying the coupling parameters g_ρ and g_δ . The symmetry energy with both the ρ and δ mesons can not be softer than one of set1 containing only ρ meson. In order to broad the range of the slope parameter, we set the slope parameter of set2 and set3 to be 109.3 and 145.0 MeV by varying the coupling parameters g_ρ and g_δ , respectively. A broader range of the slope parameter would be helpful to understand the relation between the properties of symmetry energy and the observables of heavy-ion collisions.

B. Relativistic quantum molecular dynamics approach

In order to investigate high-energy heavy-ion collision, the RQMD was proposed[39, 40]. Recently, the RMF has been implemented into the RQMD[41–43].

TABLE I: Parameter sets for RMF. The saturation density ρ_0 is set to be 0.16 fm^{-3} . The binding energy at the saturation density is $E/A - M_N = -16 \text{ MeV}$. The isoscalar-vector ω and isovector-vector ρ masses are fixed to their physical values, $m_\omega = 783 \text{ MeV}$ and $m_\rho = 763 \text{ MeV}$. The remaining meson mass m_σ is set to be 550 MeV .

model	g_σ	g_ω	$g_2 \text{ (fm}^{-1}\text{)}$	g_3	g_ρ	g_δ	$K \text{ (MeV)}$	$E_{\text{sym}}(\rho_0) \text{ (MeV)}$	$L(\rho_0) \text{ (MeV)}$
set1	8.145	7.570	31.820	28.100	4.049	-	230	31.6	85.3
set2	8.145	7.570	31.820	28.100	8.673	5.347	230	31.6	109.3
set3	8.145	7.570	31.820	28.100	11.768	7.752	230	31.6	145.0

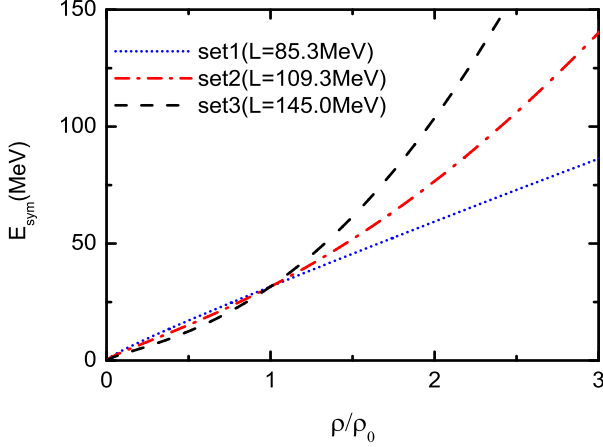


FIG. 1: (Color online) The symmetry energy as a function of the baryon density.

In RQMD, for N -body system, there are $4N$ position coordinates q_i^μ and $4N$ momentum coordinates p_i^μ ($i = 1, \dots, N$). However, the physical trajectories (\vec{q}_i and \vec{p}_i) are $6N$ for N -body system. $2N$ constraints are needed to reduce the number of dimensions from $8N$ to physical trajectories $6N$ [39–43, 49–51],

$$\phi_i \approx 0 \text{ (} i = 1, \dots, 2N \text{)}, \quad (10)$$

where $2N$ constraints satisfy the physical $6N$ phase space. The sign \approx means Dirac's weak equality. The on-mass shell conditions is able to reduces the phase space from $8N$ to $7N$ dimensions,

$$\phi_i \equiv p_i^{*2} - M_i^{*2} = (p_i - V_i)^2 - (M_N - S_i)^2 = 0, \quad (11)$$

here $i = 1, \dots, N$. The remaining N constraints are the time fixation constraints. A simple choice of the time fixation constraints, which obey the world-line condition, are written as[40, 49, 51, 52]

$$\begin{aligned} \phi_{i+N} &\equiv \hat{a} \cdot (q_i - q_N) = 0, \text{ (} i = 1, \dots, N-1 \text{)}, \\ \phi_{2N} &\equiv \hat{a} \cdot q_N - \tau = 0, \end{aligned} \quad (12)$$

where $\hat{a} = (1, \vec{0})$ is the four-dimensional unit-vector[39–43, 49]. In two-body center-of-mass system, \hat{a} is defined as $p_{ij}^\mu / \sqrt{p_{ij}^2}$ with $p_{ij}^\mu = p_i^\mu + p_j^\mu$. We see that only the constraint $i = 2N$ depends on τ . With the above $2N$ constraints, the number of dimensions $8N$ will reduce

to $6N$. These $2N$ constraints are conserved in time:

$$\begin{aligned} \frac{d\phi_i}{d\tau} &= \frac{\partial \phi_i}{\partial \tau} + \sum_k^{2N} \lambda_k [\phi_i, \phi_k] = 0 \\ &= \frac{\partial \phi_i}{\partial \tau} + \sum_k^{2N} C_{ik}^{-1} \lambda_k = 0. \end{aligned} \quad (13)$$

Since only the constraint $i = 2N$ depends on τ , λ is written as[49]

$$\lambda_i = -C_{2N,i} \frac{\partial \phi_{2N}}{\partial \tau}, \text{ (} i = 1, \dots, 2N-1 \text{)}, \quad (14)$$

with $C_{ij}^{-1} = [\phi_i, \phi_j]$. The Poisson brackets are defined as

$$[A, B] = \sum_k \left(\frac{\partial A}{\partial p_k} \cdot \frac{\partial A}{\partial q_k} - \frac{\partial B}{\partial q_k} \cdot \frac{\partial B}{\partial p_k} \right). \quad (15)$$

Follow previous studies, the Hamiltonian of the N -body system is constructed as the linear combination of $2N-1$ constraints[49, 51, 52]:

$$H = \sum_{i=1}^{2N-1} \lambda_i(\tau) \phi_i, \quad (16)$$

Assuming $[\phi_i, \phi_j] = 0$, the $\lambda_i = 0$ for $N+1 < i < 2N$ [49]. The equations of motion are then obtained as

$$\begin{aligned} \frac{dq_i}{d\tau} &= [H, q_i] = \sum_j^N \lambda_j \frac{\partial \phi_j}{\partial p_i}, \\ \frac{dp_i}{d\tau} &= [H, p_i] = - \sum_j^N \lambda_j \frac{\partial \phi_j}{\partial q_i}, \end{aligned} \quad (17)$$

with the on-mass shell conditions (Eq.(11)) as inputs, the equations of motion are obtained as

$$\begin{aligned} \dot{\vec{r}}_i &= \frac{\vec{p}_i^*}{p_i^{*0}} + \sum_{j=1}^N \left(\frac{M_j^*}{p_j^{*0}} \frac{\partial M_j^*}{\partial \vec{p}_i} + z_j^{*\mu} \cdot \frac{\partial V_{j\mu}}{\partial \vec{p}_i} \right), \\ \dot{\vec{p}}_i &= - \sum_{j=1}^N \left(\frac{M_j^*}{p_j^{*0}} \frac{\partial M_j^*}{\partial \vec{r}_i} + z_j^{*\mu} \cdot \frac{\partial V_{j\mu}}{\partial \vec{r}_i} \right), \end{aligned} \quad (18)$$

where $z_i^{*\mu} = p_i^{*\mu} / p_i^{*0}$ and $M_i^* = M_N - S_i$. The scalar potential S_i and the vector potential $V_{i\mu}$ in RQMD are written as

$$\begin{aligned} S_i &= \frac{1}{2} g_\sigma \sigma_i + \frac{1}{2} g_\delta t_i \delta_i \\ V_{i,\mu} &= \frac{B_i}{2} g_\omega \omega_{i,\mu} + \frac{B_i t_i}{2} g_\rho b_{i,\mu} \end{aligned} \quad (19)$$

here $t_i = 1$ for protons and $t_i = -1$ for neutrons. B_i is the baryon number of the i th particle. The meson field is obtained from RMF:

$$\begin{aligned} m_\sigma^2 \sigma_i + g_2 \sigma_i^2 + g_3 \sigma_i^3 &= g_\sigma \rho_{S,i}, \\ m_\omega \omega_i^\mu &= g_\omega J_i^\mu, \\ m_\delta^2 \delta_i &= g_\delta (\rho_{Sp,i} - \rho_{Sn,i}) = g_\delta \rho_{S3,i}, \\ m_\rho^2 b_i &= g_\rho (\rho_p - \rho_n) = g_\rho R_i^\mu. \end{aligned} \quad (20)$$

In the RQMD approach, the scalar density, the isovector-scalar density, the baryon current and the isovector baryon current are written as

$$\begin{aligned} \rho_{S,i} &= \sum_{j \neq i} \frac{M_j}{p_j^0} \rho_{ij}, & \rho_{S3,i} &= \sum_{j \neq i} t_j \frac{M_j}{p_j^0} \rho_{ij}, \\ J_i^\mu &= \sum_{j \neq i} B_j \frac{p_j^\mu}{p_j^0} \rho_{ij}, & R_i^\mu &= \sum_{j \neq i} t_j B_j \frac{p_j^\mu}{p_j^0} \rho_{ij}. \end{aligned} \quad (21)$$

Since the difference between the numerical results by using effective mass M_j^* and kinetic momentum $p_j^{\mu*}$ in density and current and those by using a free mass $M_j = M_N = 938$ MeV and canonical momentum p_j^μ in density and current is small, a free mass $M_j = M_N = 938$ MeV and canonical momentum p_j^μ have been used in the above density and current[42]. The interaction density ρ_{ij} is given by the Gaussian:

$$\rho_{ij} = \frac{\gamma_{ij}}{(4\pi L)^{3/2}} \exp\left(-\frac{q_{T,ij}^2}{4L}\right), \quad (22)$$

where $q_{T,ij}^2$ is a distance squared. γ_{ij} is a Lorentz factor ensuring the correct normalization of the Gaussian[53], and equals $(p_i^0 + p_j^0)/(p_i + p_j)$ in two-body center-of-mass frame. In this work, we set the square of wave-packet width as $L = 2.0 fm^2$.

C. The dispersion relation and production of pion

The Hamiltonian of mesons is defined as[44, 54–56]

$$H_M = \sum_{i=1}^{N_M} [V_i^C + \omega(\vec{p}_i, \rho_i)], \quad (23)$$

V_i^C is the Coulomb potential, and is written as

$$V_i^C = \sum_{j=1}^{N_B} \frac{e_i e_j}{r_{ij}}, \quad (24)$$

N_M and N_B are the total numbers of mesons and baryons including charged resonances, respectively. The pion potential in the medium, which contains the isoscalar and isovector contributions, is defined as

$$\omega(\vec{p}_i, \rho_i) = \omega_{isoscalar}(\vec{p}_i, \rho_i) + C_\pi \tau_z \alpha (\rho/\rho_0)^{\gamma_\pi}, \quad (25)$$

where α is the isospin asymmetry parameter. The coefficient C_π equals 36 MeV. The isospin quantity τ is 1, 0 and -1 for π^- , π^0 and π^+ , respectively. γ_π determines the isospin splitting of pion potential, and is set

to be 2. In this work, the scalar part of pion potential $\omega_{isoscalar}$ is chosen as the Δ -hole model. The pion potential, which contains a pion branch (smaller value) and a Δ -hole (larger value) branch, is defined as

$$\begin{aligned} \omega_{isoscalar}(\vec{p}_i, \rho_i) &= S_\pi(\vec{p}_i, \rho_i) \omega_{\pi-like}(\vec{p}_i, \rho_i) + \\ &S_\Delta(\vec{p}_i, \rho_i) \omega_{\Delta-like}(\vec{p}_i, \rho_i). \end{aligned} \quad (26)$$

The probability of the pion branch and the Δ -hole branch satisfies the following equation:

$$S_\pi(\vec{p}_i, \rho_i) + S_\Delta(\vec{p}_i, \rho_i) = 1, \quad (27)$$

The probability of both the pion branch and the Δ -hole branch is defined as[56]

$$S(\vec{p}_i, \rho_i) = \frac{1}{1 - \partial \Pi(\omega)/\partial \omega^2}, \quad (28)$$

where ω stands for $\omega_{\pi-like}$ and $\omega_{\Delta-like}$. The eigenvalues of $\omega_{\pi-like}$ and $\omega_{\Delta-like}$ are generated from the pion dispersion relation:

$$\omega^2 = \vec{p}_i^2 + m_\pi^2 + \Pi(\omega), \quad (29)$$

where Π is the pion self-energy. Including the short-range Δ -hole interaction, the pion self-energy is defined as

$$\Pi = \frac{\vec{p}_i^2 \chi}{1 - g' \chi}, \quad (30)$$

here m_π is the pion mass. The Migdal parameter g' is set to be 0.6. χ is defined as

$$\chi = -\frac{8}{9} \left(\frac{f_\Delta}{m_\pi}\right)^2 \frac{\omega_\Delta \rho \hbar^3}{\omega_\Delta^2 - \omega^2} \exp(-2\vec{p}_i^2/b^2), \quad (31)$$

where $\omega_\Delta = \sqrt{m_\Delta^2 + \vec{p}_i^2} - M_N$, and m_Δ is the delta masses. In this work, the $\pi N \Delta$ coupling constant f_Δ is 2, and the cutoff factor b is $7m_\pi$.

In this work, we assume that the mass and energy-momentum of Δ resonances are not changed by the RMF, and neglect the threshold effect[57–59]. With the energy of pion and Coulomb potential, the energy balance of this work in the decay of resonances is written as:

$$\sqrt{m_R^2 + \vec{p}_R^2} = \sqrt{M_N^2 + (\vec{p}_R - \vec{p}_\pi)^2} + \omega_\pi(\vec{p}_\pi, \rho) + V_\pi^C, \quad (32)$$

where \vec{p}_R and \vec{p}_π are the momenta of resonances and pions, respectively. m_R is the mass of resonances.

The pion is generated from the direct nucleon-nucleon collision and decay of the resonances $\Delta(1232)$ and $N^*(1440)$. The relation channels of resonances and pions, which are taken as same as those of LQMD model, are given as follow[31, 44, 60, 61]:

$$\begin{aligned} NN &\leftrightarrow N\Delta, & NN &\leftrightarrow NN^*, & NN &\leftrightarrow \Delta\Delta, & \Delta &\leftrightarrow N\pi, \\ N^* &\leftrightarrow N\pi, & NN &\rightarrow NN\pi(s-state). \end{aligned} \quad (33)$$

For the production of $\Delta(1232)$ and $N^*(1440)$ resonances in a nucleon-nucleon scattering, the parameterized cross

section calculated by the one-boson exchange model has been employed[62]. The decay width of $\Delta(1232)$ and $N^*(1440)$, which originates from the p-wave resonances, is momentum-dependent and expressed as[62]

$$\Gamma(|\vec{p}|) = \frac{a_1 |\vec{p}|^3}{(1 + a_2 |\vec{p}|^2)(a_3 + |\vec{p}|^2)} \Gamma_0, \quad (34)$$

where $|\vec{p}|$ is the momentum of the created pion. The parameters a_1 , a_2 and a_3 are taken as 22.48 (17.22), 39.69 (39.69), 0.04(0.09) for $\Delta(N^*)$, respectively. The bare decay width of $\Delta(N^*)$ is given as $\Gamma_0 = 0.12(0.2)\text{GeV}$. With the momentum-dependent decay width, the cross section of pion-nucleon scattering has the Breit-Wigner form:

$$\sigma_{\pi N}(\sqrt{s}) = \sigma_{\max} \left(\frac{\vec{p}_0}{\vec{p}} \right)^2 \frac{0.25\Gamma^2(\vec{p})}{0.25\Gamma^2(\vec{p}) + (\sqrt{s} - m_0)^2}, \quad (35)$$

where \vec{p} and \vec{p}_0 are the three-momenta of pions at energy of \sqrt{s} and m_0 , respectively. The maximum cross section σ_{\max} of Δ and N^* resonances is obtained by fitting the total cross sections of the experimental data in pion-nucleon scattering with the Breit-Wigner formula[63]. For instance, the maximum cross section σ_{\max} of Δ resonance is 200, 133.33, and 66.7 mb for $\pi^+p \rightarrow \Delta^{++}$ ($\pi^-n \rightarrow \Delta^-$), $\pi^0p \rightarrow \Delta^+$ ($\pi^0n \rightarrow \Delta^0$) and $\pi^-p \rightarrow \Delta^0$ ($\pi^+n \rightarrow \Delta^+$), respectively[61].

III. RESULTS AND DISCUSSIONS

We have implemented the RMF model into the LQMD model. To check this model, we first investigate the collective flows of $^{108}\text{Sn} + ^{112}\text{Sn}$ and $^{132}\text{Sn} + ^{124}\text{Sn}$ collisions. The directed and elliptic flows come from the Fourier expansion of the azimuthal distribution:

$$\frac{dN}{d\phi}(y, p_T) = N_0 [1 + 2V_1(y, p_T)\cos(\phi) + 2V_2(y, p_T)\cos(2\phi)], \quad (36)$$

where the azimuthal angle of the emitted particle ϕ is measured from the reaction plane. $p_T = \sqrt{p_x^2 + p_y^2}$ is the transverse momentum. The directed flow V_1 and elliptic flow V_2 are written as

$$V_1 \equiv \langle \cos(\phi) \rangle = \langle \frac{p_x}{p_T} \rangle, \\ V_2 \equiv \langle \cos(2\phi) \rangle = \langle \frac{p_x^2 - p_y^2}{p_T^2} \rangle, \quad (37)$$

The directed flow stands for information on the azimuthal anisotropy of the transverse emission. The elliptic flow tells us about the competition between the in-plane ($V_2 > 0$) and out-of-plane $V_2 < 0$ emissions. Since interactions of nuclear matter will have impact on collective flows, the collective flows have been used to extract the high-density behavior of the EOS widely.

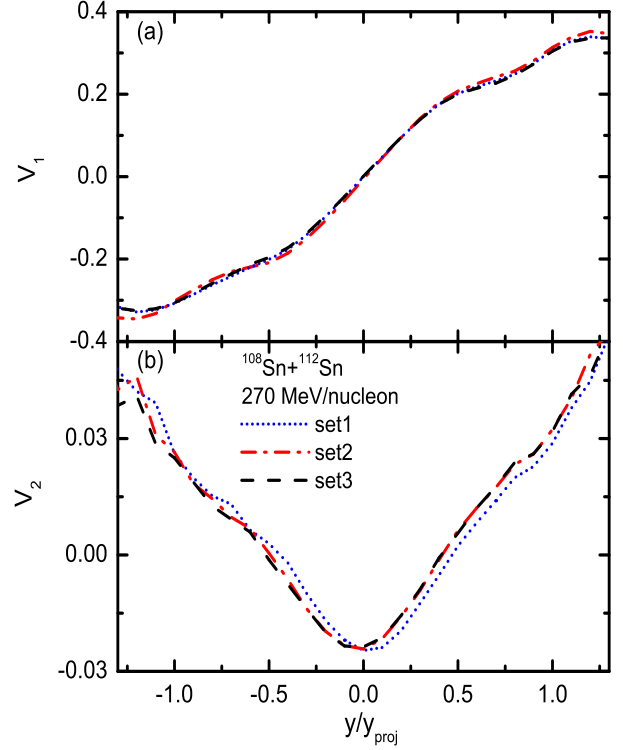


FIG. 2: (Color online) Rapidity distribution of the collective flows of free neutrons in the $^{108}\text{Sn} + ^{112}\text{Sn}$ reaction at an incident energy of 270 MeV/nucleon for impact parameter $b=3$ fm.

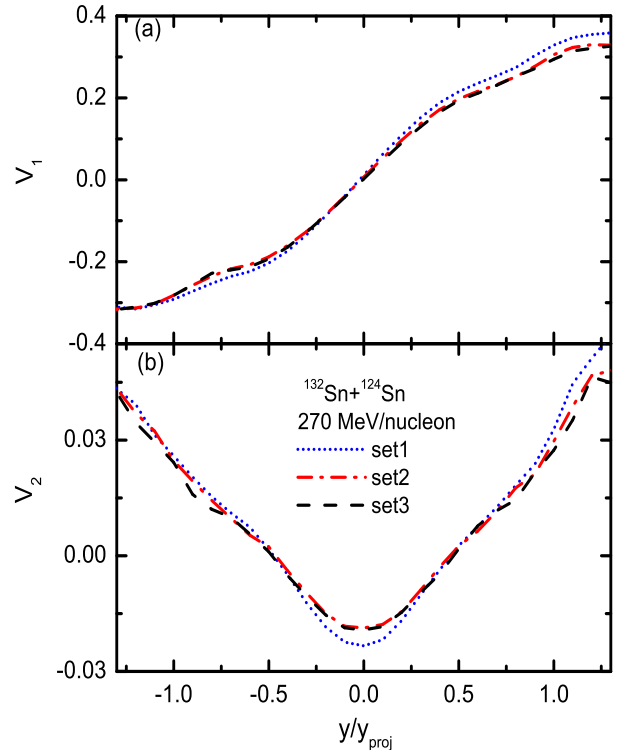


FIG. 3: (Color online) Rapidity distribution of the collective flows of free neutrons in the $^{132}\text{Sn} + ^{124}\text{Sn}$ reaction at an incident energy of 270 MeV/nucleon for impact parameter $b=3$ fm.

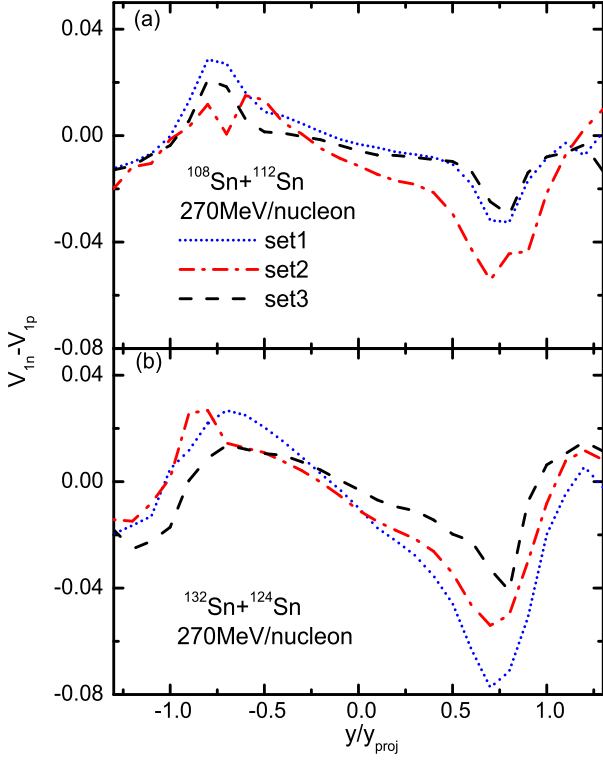


FIG. 4: (Color online) The difference between neutron and proton directed flows in the $^{108}\text{Sn} + ^{112}\text{Sn}$ and $^{132}\text{Sn} + ^{124}\text{Sn}$ reactions at an incident energy of 270 MeV/nucleon.

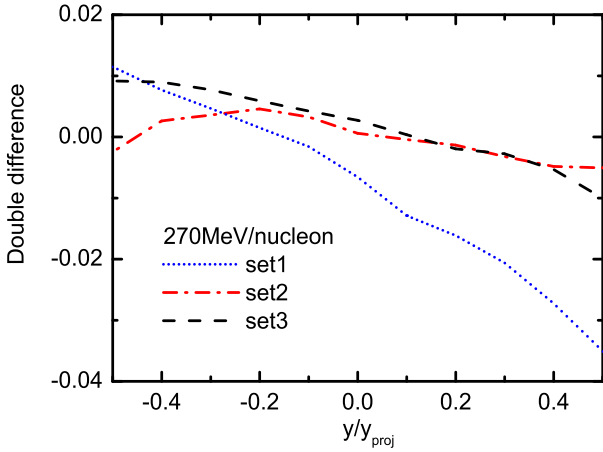


FIG. 5: (Color online) The double difference of directed flows $(V_{1n} - V_{1p})_{^{132}\text{Sn} + ^{124}\text{Sn}} - (V_{1n} - V_{1p})_{^{108}\text{Sn} + ^{112}\text{Sn}}$ at an incident energy of 270 MeV/nucleon.

The $^{108}\text{Sn} + ^{112}\text{Sn}$ and $^{132}\text{Sn} + ^{124}\text{Sn}$ collisions of this work are investigated at the incident energies of 270 A MeV and impact parameter $b=3$ fm. At incident energies of 270 A MeV, the nuclear matter of collision central can be compressed to densities approaching $2\rho_0$. At this dense region, the collective flows, which reflect the repulsion interaction, may depend on the slope of symmetry energy. The directed and elliptic flows of $^{108}\text{Sn} + ^{112}\text{Sn}$ are shown in Fig.2, and the directed and elliptic flows of $^{132}\text{Sn} + ^{124}\text{Sn}$ are shown in Fig.3. It is reasonable that the directed flow V_1 is an order of

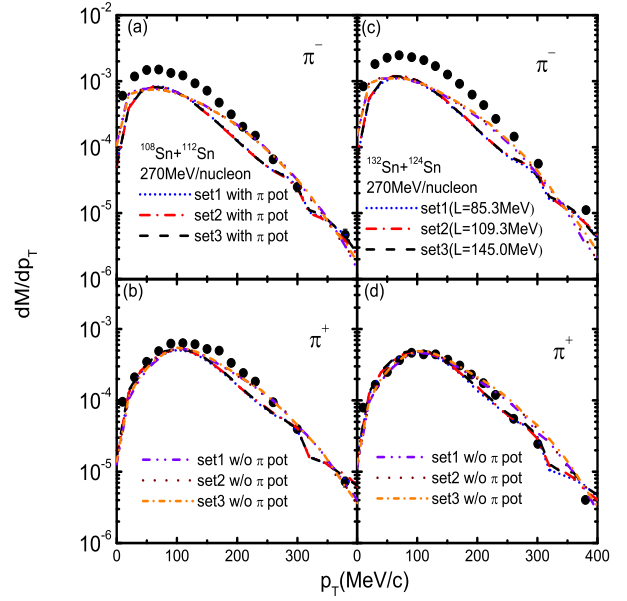


FIG. 6: (Color online) The transverse momentum spectra of pion as a function of transverse momentum at an incident energy of 270 MeV/nucleon. The left two panels [(a) and (b)] are the results of $^{108}\text{Sn} + ^{112}\text{Sn}$ reaction, and the right two panels [(c) and (d)] are the results of $^{132}\text{Sn} + ^{124}\text{Sn}$ reaction.

magnitude larger than the elliptic flow V_2 . In the same reaction system, the difference of directed flows with various slope of symmetry energy (set1, set2 and set3) is small. The difference of elliptic flows with various slope of symmetry energy is also small. In order to find the relationship between the slope of symmetric energy and the collective flow, we need to do some processing on the data of collective flow.

It has been realized that the difference between the neutron and proton directed flows emitted from heavy-ion collisions can be used to extract the density dependence of symmetry energy. The difference between the neutron and proton directed flows is defined as $V_{1n} - V_{1p}$. The difference between the neutron and proton directed flows of $^{108}\text{Sn} + ^{112}\text{Sn}$ and $^{132}\text{Sn} + ^{124}\text{Sn}$ collisions is shown in Fig.4. It is worth mentioning that the trend and shape of the difference between the neutron and proton directed flows is similar to previous study[60]. For a given single reaction system (nearly symmetric $^{108}\text{Sn} + ^{112}\text{Sn}$ system or neutron rich $^{132}\text{Sn} + ^{124}\text{Sn}$ system), the difference between the neutron and proton directed flows seems to be disorganized. When the difference between the neutron and proton directed flows of the nearly symmetric and neutron rich systems are compared side by side, the difference between soft symmetry energy and stiff symmetry energy in the neutron-rich system is inverted slightly from the more symmetric system. Therefore, we define a double difference of directed flows as $(V_{1n} - V_{1p})_{^{132}\text{Sn} + ^{124}\text{Sn}} - (V_{1n} - V_{1p})_{^{108}\text{Sn} + ^{112}\text{Sn}}$. As shown in Fig.5, the double difference of directed flows increases with increasing the slope of symmetry energy in the midrapidity region.

Apart from the collective flows, the production of isospin exotic particles, such as hyperons, kaons and pions, can also be used to extract the symmetry energy[20–26]. Since incident energy of 270 A MeV is much smaller than the threshold energy of hyperons and kaons, the isospin exotic particles are mainly pions. In this work, we calculate the properties of pion in two cases. One is to calculate properties of pion with π potential, and the other is to calculate properties of pion without π potential. As shown in Fig.6, the left and right panels are the transverse momentum spectra of pion for the nearly symmetric $^{108}\text{Sn} + ^{112}\text{Sn}$ and the neutron rich $^{132}\text{Sn} + ^{124}\text{Sn}$ reactions at $\theta_{cm} < 90^\circ$, respectively. For collisions between isotopes, the π^+ is mainly generated from the collisions between protons, and the π^- is mainly generated from the collisions between neutrons. Since the number of protons is the same for isotopes, there will be no significant difference in the yield of π^+ . As shown in lower panels (b) and (d) of Fig.6, the transverse momentum spectra of π^+ is close to each other for various systems and slopes of symmetry energy. However, since there are more neutron-neutron scatterings in neutron-rich system, there is a difference between the nearly symmetric $^{108}\text{Sn} + ^{112}\text{Sn}$ system and the neutron rich $^{132}\text{Sn} + ^{124}\text{Sn}$ system. As shown in upper panels (a) and (c) of Fig.6, the transverse momentum spectra of π^- in the neutron rich $^{132}\text{Sn} + ^{124}\text{Sn}$ system is higher than one in the nearly symmetric $^{108}\text{Sn} + ^{112}\text{Sn}$ system. Besides, theoretically, a stiffer symmetry would have a stronger repulsive force to push out neutrons resulting in decreasing the π^- yield. However, in this work, the transverse momentum spectra of π^- is not sensitive to the slope of symmetry energy. This result may be due to the fact that the symmetry energy of various slope parameter does not differ greatly at densities less than $2\rho_0$. Moreover, π^+ is consistent with the S π RIT data[37], however, the transverse momentum spectra π^- is lower than the S π RIT data. As shown in Fig.6, the effect of π potential on the transverse momentum spectra of π is obvious. The π potential in the medium, which is not well understood up to now, may be the reason why the predictions of π^- is lower than the experiment data.

For a given symmetry energy, since the symmetry potential energy is repulsive for neutrons and π^- and attractive for protons and π^+ in the neutron-rich matter, the single ratio $\text{SR}(\pi^-/\pi^+) = [dM(\pi^-)/dp_T]/[dM(\pi^+)/dp_T]$ may obviously differ for the nearly and the neutron rich systems. As shown in Fig.7, the single ratio of the neutron rich $^{132}\text{Sn} + ^{124}\text{Sn}$ system is higher than one of the nearly symmetric $^{108}\text{Sn} + ^{112}\text{Sn}$ system. However, the single ratio of this work is not sensitive to the slope of symmetry energy for a given nearly symmetric system or neutron rich system. This is mainly originated from the fact that the difference of symmetry energy with set1, set2 and set3 is not obvious at density below $2\rho_0$. Moreover, the single ratio of $^{108}\text{Sn} + ^{112}\text{Sn}$ is lower than but not far away from the experiment data at $p_T < 200$ MeV/c, and is consistent with the experiment data at $p_T > 200$ MeV/c. However, the single ratio of

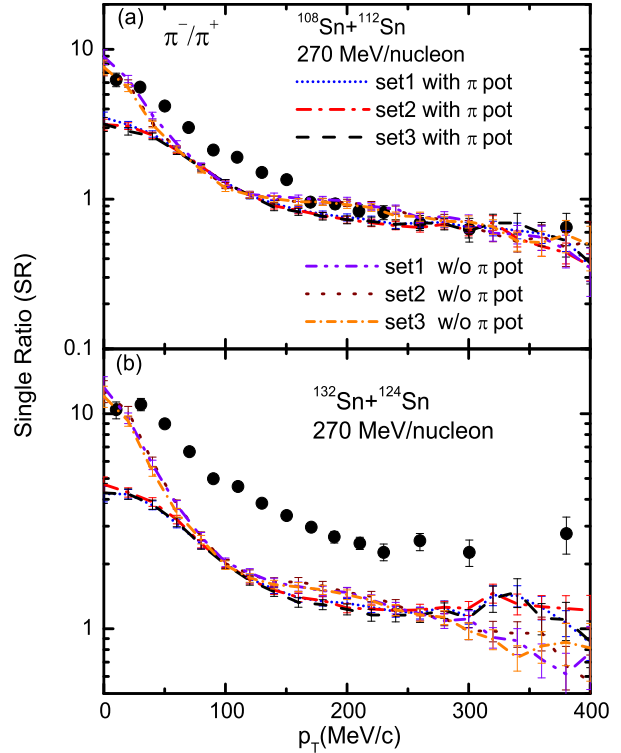


FIG. 7: (Color online) Single spectral ratios of pion as a function of transverse momentum for the $^{108}\text{Sn} + ^{112}\text{Sn}$ and $^{132}\text{Sn} + ^{124}\text{Sn}$ reactions at an incident energy of 270 MeV/nucleon.

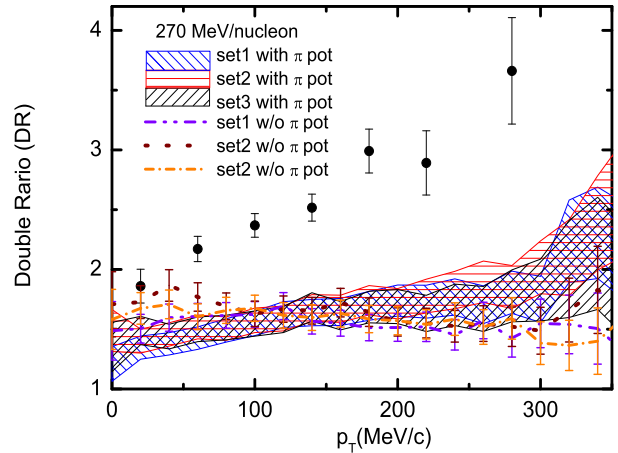


FIG. 8: (Color online) The double ratio of pion as a function of transverse momentum at an incident energy of 270 MeV/nucleon.

$^{132}\text{Sn} + ^{124}\text{Sn}$ is lower than the experimental data at the entire p_T domain. This is due to the fact that the transverse momentum spectra π^- of $^{132}\text{Sn} + ^{124}\text{Sn}$ is lower than the experiment data.

The double ratio between the neutron rich system and the nearly symmetric system $\text{DR}(\pi^-/\pi^+) = \text{SR}(\pi^-/\pi^+)_{132+124}/\text{SR}(\pi^-/\pi^+)_{108+112}$, which can cancel out most of the systematic errors caused by Coulomb and isoscalar interactions, is thought to be sensitive to the properties of the symmetry energy. However, as

shown in Fig.8, with considering the π potential, the double ratios of various slope parameters (set1, set2 and set3) are overlapping with each other. This is due to the fact that the symmetry energy of set1, set2 and set3 is similar to each at density below $2\rho_0$. The double ratio without the π potential decreases with increasing the transverse momentum, however, the double ratio with the π potential increases with increasing the transverse momentum. The increasing trend of double ratio without π potential energy is opposite to one of the experimental results, however, the increasing trend of double ratio with π potential energy is consistent with one of the experimental results. Therefore, when the understanding of the π potential in the medium becomes clear, the double ratio can be used to extract the properties of symmetry energy.

IV. CONCLUSIONS

The RMF with the different slope parameter of symmetry energy, namely set1, set2 and set3, has been implemented into the LQMD transport model. The collective flows of the nearly symmetric $^{108}\text{Sn} + ^{112}\text{Sn}$ and the neutron rich $^{132}\text{Sn} + ^{124}\text{Sn}$ systems have been successfully generated from the LQMD.RMF. It has been observed that the directed flow V_1 is an order of magnitude larger than the elliptic flow V_2 . For a given system, the directed flow V_1 and the elliptic flow V_2 are close to each other for various slopes of symmetry energy. To explore the relationship between the collective flow and the slope of the symmetric energy, we have defined a difference between the neutron and proton directed flows $V_{1n} - V_{1p}$ and a double difference $(V_{1n} - V_{1p})_{^{132}\text{Sn} + ^{124}\text{Sn}} - (V_{1n} - V_{1p})_{^{108}\text{Sn} + ^{112}\text{Sn}}$. When the difference between the neutron and proton directed flows of the nearly symmetric and neutron rich systems are compared side by side, it is found that the double difference of directed flows increases with

increasing the slope of symmetry energy in the midrapidity region.

We also investigate the relationship between the isospin exotic particles and the symmetry energy. At incident energies of 270 A MeV, since the generation threshold of hyperons and kaons is not reached, the isospin exotic particles are pions in this work. The transverse momentum spectra of π^+ is consistent with the experiment data, however, the transverse momentum spectra of π^- is a little lower than the experiment data. This lower transverse momentum spectra of π^- will cause lower single ratio and lower double ratio than the experiment data. The lower transverse momentum spectra of π^- may be due to the poor understanding of the π potential in the medium. For given reaction system, the transverse momentum spectra of π^+ and π^- is almost the same for various slopes of symmetry energy in this work. As a consequence, the single ratio and the double ratio are also similar to each other. This is due to the fact that the symmetry energy of set1, set2 and set3 is similar to each at density below $2\rho_0$. The effect of π potential on the properties of π is obvious. Especially, the double ratio without the π potential decreases with increasing the transverse momentum, however, the double ratio with the π potential increases with increasing the transverse momentum. When the understanding of the π potential in the medium becomes clear, we believe that the properties of isospin exotic particles can be used to extract the symmetry energy.

ACKNOWLEDGMENT

This work was supported by the National Natural Science Foundation of China (Projects Nos 12147106, 12175072 and 11722546) and the Talent Program of South China University of Technology (Projects No. 20210115).

-
- [1] P. Danielewicz, R. Lacey, and W. G. Lynch, Science, **298**, 1592(2002).
 - [2] B. P. Abbott, R. Abbott, T. D. Abbott, F. Acernese, K. Ackley, and C. Adams, *et al.*, Phys. Rev. Lett. **121**, 161101 (2018).
 - [3] S. Huth, P. T. H. Pang, I. Tews, T. Dietrich, A. Le Fevre, and A. Schwenk, *et al.*, Nature **606**, 276-280 (2022).
 - [4] L. W. Chen, Nucl. Phys. Rev., **34**, 20-28(2017).
 - [5] B. A. Li, P. G. Krastev, D. H. Wen, and N. B. Zhang, Eur. Phys. J. A, **55**, 117(2019).
 - [6] B. T. Reed, F. J. Fattoyev, C. J. Horowitz, and J. Piekarewicz, Phys. Rev. Lett. **126**, 172503(2021).
 - [7] J. M. Lattimer, and M. Prakash Science, **442**, 109-165 (2007).
 - [8] A. Drago, A. Lavagno, G. Pagliara, and D. Pigato, Phys. Rev. C **90**, 065809 (2014).
 - [9] J. M. Lattimer and M. Prakash, Phys. Rep. **621**, 127 (2016).
 - [10] M. Tsang, W. Lynch, P. Danielewicz, and C. Tsang, Phys. Lett. B **795**, 533 (2019).
 - [11] B. Fore and S. Reddy, Phys. Rev. C **101**, 035809 (2020).
 - [12] W. Scheid, H. Müller, and W. Greiner, Phys. Rev. Lett. **32**, 741 (1974).
 - [13] J. Kapusta and D. Strottman, Phys. Lett. B **106**, 33 (1981).
 - [14] H. Stöcker, L. P. Csernai, G. Graebner, G. Buchwald, H. Kruse, R. Y. Cusson, J. A. Maruhn, and W. Greiner, Phys. Rev. C **25**, 1873 (1982).
 - [15] H. A. Gustafsson, H. H. Gutbrod, B. Kolb, H. Lohner, B. Ludewigt, A. M. Poskanzer, T. Renner, H. Riedesel, H. G. Ritter, A. Warwick, F. Weik, and H. Wieman, Phys. Rev. Lett. **52**, 1590 (1984).
 - [16] D. H. Rischke, Y. Poursun, J. A. Maruhn, H. Stoecker, and W. Greiner, Acta Phys. Hung. A **1**, 309 (1995).
 - [17] J. Brachmann, S. Soff, A. Dumitru, H. Stöcker, J. A. Maruhn, W. Greiner, L. V. Bravina, and D. H. Rischke, Phys. Rev. C **61**, 024909 (2000).
 - [18] L. P. Csernai and D. Rohrich, Phys. Lett. B **458**, 454 (1999).

- [19] B. A. Li and C. M. Ko, Phys. Rev. C **58**, R1382 (1998).
 [20] L. Scalone, M. Colonna, and M. Di Toro, Phys. Lett. B **461**, 9 (1999).
 [21] B. A. Li, A. T. Sustich, and B. Zhang, Phys. Rev. C **64**, 054604 (2001).
 [22] Q. F. Li, C. W. Shen, C. C. Guo, Y. J. Wang, Z. X. Li, J. Lukasik, and W. Trautmann, Phys. Rev. C **83**, 044617 (2011).
 [23] M. D. Cozma, Phys. Lett. B **700**, 139 (2011).
 [24] G. Ferini, T. Gaitanos, M. Colonna, M. Di Toro, and H. H. Wolter, Phys. Rev. Lett. **97**, 202301 (2006).
 [25] B. A. Li, Phys. Rev. Lett. **88**, 192701 (2002).
 [26] T. Gaitanos, M. Di Toro, S. Typel, V. Baran, C. Fuchs, V. Greco, and H. H. Wolter, Nucl. Phys. A **732**, 24 (2004).
 [27] C. Sturm, I. Bottcher, M. Debowski, A. Forster, E. Grosse, P. Koczon, and B. Kohlmeier, *et al.*, (KaoS Collaboration), Phys. Rev. Lett. **86**, 39 (2001).
 [28] G. Q. Li and C. M. Ko, Phys. Lett. B **349**, 405 (1995).
 [29] C. Fuchs, A. Faessler, E. Zabrodin, and Y. M. Zheng, Phys. Rev. Lett. **86**, 1974 (2001).
 [30] C. Hartnack, H. Oeschler, and J. Aichelin, Phys. Rev. Lett. **96**, 012302 (2006).
 [31] Z. Q. Feng, Phys. Rev. C **83**, 067604 (2011).
 [32] Z. Q. Feng and G. M. Jin, Phys. Lett. B **683**, 140 (2010).
 [33] P. Russotto, P. Z. Wu, M. Zoric, M. Chartier, Y. Leifels, R. C. Lemmon, and Q. Li, *et al.*, Phys. Lett. B **697**, 471 (2011).
 [34] Z. G. Xiao, B. A. Li, L. W. Chen, G. C. Yong, and M. Zhang, Phys. Rev. Lett. **102**, 062502 (2009).
 [35] W. J. Xie, J. Su, L. Zhu, and F. S. Zhang, Phys. Lett. B **718**, 1510 (2013).
 [36] W. Reisdorf, M. Stockmeier, A. Andronic, M. L. Benabderrahmane, O. N. Hartmann, and N. Herrmann, *et al.*, Nucl. Phys. A **781**, 459 (2007).
 [37] G. Jhang, J. Estee, J. Barney, G. Cerizza, and M. Kaneko, *et al.*, Phys. Lett. B **813**, 136016 (2021).
 [38] J. Estee, W.G. Lynch, C.Y. Tsang, J. Barney, G. Jhang, M.B. Tsang, and R. Wang, *et al.*, Phys. Rev. Lett. **126**, 162701 (2021).
 [39] H. Sorge, H. Stöcker, and W. Greiner, Ann. Phys. **192**, 266 (1989).
 [40] T. Maruyama, S. W. Huang, N. Ohtsuka, G. Li, and A. Faessler, Nucl. Phys. A **534**, 720 (1991).
 [41] Y. Nara and H. Stoecker, Phys. Rev. C **100**, 054902 (2019).
 [42] Y. Nara, T. Maruyama, and H. Stoecker, Phys. Rev. C **102**, 024913 (2020).
 [43] Y. Nara, A. Jinno, K. Murase, and A. Ohnishi, Phys. Rev. C **106**, 044902 (2022).
 [44] Z. Q. Feng, W. J. Xie, P. H. Chen, J. Chen, and G. M. Jin, Phys. Rev. C **92**, 044604 (2015).
 [45] J. D. Walecka, Ann. Phys. **83**, 491 (1974).
 [46] J. Boguta, and A. R. Bodmer, Nucl. Phys. A **292**, 413 (1977).
 [47] B. D. Serot, Phys. Lett. B **86B**, 146 (1979).
 [48] S. Kubis, and M. Kutschera, Phys. Lett. B **399**, 191 (1997).
 [49] R. Marty, and J. Aichelin, Phys. Rev. C **87**, 034912 (2013).
 [50] A. Komar, Phys. Rev. D **18**, 1881 (1978).
 [51] M. Isse, A. Ohnishi, N. Otuka, P. K. Sahu, and Y. Nara, Phys. Rev. C **72**, 064908 (2005).
 [52] E. C. G. Sudarshan, N. Mukunda, and J. N. Goldberg, Phys. Rev. D **23**, 2218 (1981).
 [53] D. Oliinychenko, and H. Petersen, Phys. Rev. C **93**, 034905 (2016).
 [54] G. E. Brown and W. Weise, Phys. Rep. **22**, 279 (1975).
 [55] B. Friemann, V. P. Pandharipande, and Q. N. Usmani, Nucl. Phys. A **372**, 483 (1981).
 [56] L. Xiong, C. M. Ko, and V. Koch, Phys. Rev. C **47**, 788 (1993).
 [57] G. Ferini, M. Colonna, T. Gaitanos, and M. Di Toro, Nucl. Phys. A **762**, 147 (2005).
 [58] T. Song, and C. M. Ko, Phys. Rev. C **91**, 014901 (2015).
 [59] M.D. Cozma, Phys. Lett. B **753**, 166-172 (2016).
 [60] Z. Q. Feng, Phys. Rev. C **85**, 014604 (2012).
 [61] Z. Q. Feng, Phys. Rev. C **94**, 054617 (2016).
 [62] S. Huber, and J. Aichelin, Nucl. Phys. A **573**, 587 (1994).
 [63] B. A. Li, A. T. Sustich, B. Zhang, and C. M. Ko, Int. J. Mod. Phys. E **10**, 267 (2001).

Appendix A: DETAILS of EQUATION OF MOTION

For numerical calculation, the equation of motion (Eq.(18)) needs to be written in computed form. With Eq.(19) and $M_i^* = M_i - S_i = M_N - S_i$ as inputs, the equation of motion (Eq.(18)) can be expanded as

$$\begin{aligned} \dot{\vec{r}}_i = & \frac{\vec{p}_i^*}{p_i^{*0}} + \sum_{j \neq i} [D_{ij} \frac{\partial \rho_{ij}}{\partial \vec{p}_i} + D_{ji} \frac{\partial \rho_{ji}}{\partial \vec{p}_i} \\ & + (D_j^\mu \frac{\partial f_i}{\partial \vec{p}_i} + A_{ji}^\mu \frac{\partial z_{i\mu}}{\partial \vec{p}_i}) \rho_{ji} \\ & + (D_j' t_i \frac{\partial f_i}{\partial \vec{p}_i} + A_{ji}'^\mu \frac{\partial z_{i\mu}}{\partial \vec{p}_i}) \rho_{ji}], \end{aligned} \quad (\text{A1})$$

$$\vec{p} = - \sum_{j \neq i} [D_{ij} \frac{\partial \rho_{ij}}{\partial \vec{r}_i} + D_{ji} \frac{\partial \rho_{ji}}{\partial \vec{r}_i}], \quad (\text{A2})$$

with

$$D_{ij} = D_i f_j + A_{ij}^\mu z_{j\mu} + D_i' t_j f_j + A_{ij}'^\mu z_{j\mu} \quad (\text{A3})$$

$$D_i = - \frac{g_\sigma M_i^*}{2} \frac{\partial \sigma_i}{p_i^{*0} \partial \rho_{Si}} \quad (\text{A4})$$

$$A_{ij}^\mu = \frac{g_\omega^2}{2m_\omega^2} B_i B_j z_i^{*\mu} \quad (\text{A5})$$

$$D_i' = - \frac{g_\delta}{2} t_i \frac{M_i^*}{p_i^{*0}} \frac{\partial \delta_i}{\partial \rho_{S3,i}} \quad (\text{A6})$$

$$A_{ij}'^\mu = \frac{g_\rho^2}{2m_\rho^2} t_i t_j B_i B_j z_i^{*\mu} \quad (\text{A7})$$

where $z_i^\mu = p_i^\mu / p_i^0$ and $z_i^{*\mu} = p_i^{*\mu} / p_i^{*0}$. Based on Eq.(20), $\frac{\partial \sigma_i}{\partial \rho_{Si}}$ and $\frac{\partial \delta_i}{\partial \rho_{S3,i}}$ are obtained as follow:

$$\frac{\partial \sigma_i}{\partial \rho_{Si}} = \frac{g_\sigma}{m_\sigma^2 + 2g_2 \sigma_i + 3g_3 \sigma_i^2}, \quad \frac{\partial \delta_i}{\partial \rho_{S3,i}} = \frac{g_\delta}{m_\delta^2} \quad (\text{A8})$$

In two-body center-of-mass frame, ρ_{ij} equals ρ_{ji} . The distance squared $q_{T,ij}^2$ reduces to $q_{T,ij}^2 \equiv -\vec{r}_{ij}^2 -$

$\frac{(\vec{r}_{ij} \cdot \vec{p}_{ij})^2}{p_{ij}^2}$. In actual calculation, we have replaced p_i^0 with $\sqrt{\vec{p}_i^2 + M_i^2}$ to save calculation time[51]. In doing so, the partial derivative of density versus momentum and space can be written as

$$\begin{aligned} \frac{\partial \rho_{ij}}{\partial \vec{p}_i} = & -\frac{\rho_{ij}}{2L} \frac{(\vec{r}_{ij} \cdot \vec{p}_{ij}) \cdot \vec{r}_{ij}}{p_{ij}^2} - \frac{\rho_{ij}}{2L} \frac{(\vec{r}_{ij} \cdot \vec{p}_{ij})^2}{p_{ij}^4} \left\{ \vec{p}_{ij} - \frac{\vec{p}_i}{p_i^0} p_{ij}^0 \right\} \\ & + \rho_{ij} \frac{\gamma_{ij}^2 \vec{\beta}_{ij}}{p_i^0 + p_j^0} \left[1 - \vec{\beta}_{ij} \frac{\vec{p}_i}{p_i^0} \right], \end{aligned} \quad (\text{A9})$$

$$\frac{\partial \rho_{ij}}{\partial \vec{r}_i} = -\frac{\rho_{ij}}{2L} [\vec{r}_{ij} + \frac{(\vec{r}_{ij} \cdot \vec{p}_{ij}) \cdot \vec{p}_{ij}}{p_{ij}^2}], \quad (\text{A10})$$

where $\vec{\beta}_{ij}$ is defined as $(\vec{p}_i + \vec{p}_j)/(p_i^0 + p_j^0)$. Besides, $\frac{\partial f_i}{\partial \vec{p}_i}$ can be written as $-\frac{M_i \vec{p}_i}{p_i^3}$. The partial derivative of energy part of $\frac{\partial z_{i\mu}}{\partial \vec{p}_i}$ is zero, and the partial derivative of momentum part of $\frac{\partial z_{i\mu}}{\partial \vec{p}_i}$ is written as $\frac{-p_i^2}{p_i^{03}}$. With those above equations, the momentum and space of neutrons and protons are known for sure.